# Selectivity and self-assembly in the control of a bacterial toxin by an antitoxic noncoding RNA pseudoknot

Francesca L. Short, Xue Y. Pei, Tim R. Blower[1], Shue-Li Ong, Peter C. Fineran[2], Ben F. Luisi, and George P. C. Salmond[3]

Department of Biochemistry, University of Cambridge, Cambridge, CB2 1QW, United Kingdom

Edited by Susan Gottesman, National Institutes of Health, Bethesda, MD, and approved November 27, 2012 (received for review September 17, 2012)

**Bacterial small RNAs perform numerous regulatory roles, including acting as antitoxic components in toxin–antitoxin systems. In type III toxin–antitoxin systems, small processed RNAs directly antagonize their toxin protein partners, and in the systems characterized the toxin and antitoxin components together form a trimeric assembly. In the present study, we sought to define how the RNA antitoxin, ToxI, inhibits its potentially lethal protein partner, ToxN. We show through cross-inhibition experiments with the ToxIN systems from *Pectobacterium atrosepticum* ($ToxIN_{Pa}$) and *Bacillus thuringiensis* ($ToxIN_{Bt}$) that ToxI RNAs are highly selective enzyme inhibitors. Both systems have an "addictive" plasmid maintenance phenotype. We demonstrate that $ToxI_{Pa}$ can inhibit $ToxN_{Pa}$ in vitro both in its processed form and as a repetitive precursor RNA, and this inhibition is linked to the self-assembly of the trimeric complex. Inhibition and self-assembly are both mediated entirely by the $ToxI_{Pa}$ RNA, with no requirement for cellular factors or exogenous energy. Finally, we explain the origins of ToxI antitoxin selectivity through our crystal structure of the $ToxIN_{Bt}$ complex. Our results show how a processed RNA pseudoknot can inhibit a deleterious protein with exquisite molecular specificity and how these self-contained and addictive RNA-protein pairs can confer different adaptive benefits in their bacterial hosts.**

RNA inhibition | mRNA interferase | RNA-protein complex | abortive infection | plasmid stabilization

Bacteria possess an extensive set of small, noncoding RNAs, which are used in housekeeping, regulatory, and defensive roles (1). The majority of bacterial small RNAs act at the mRNA level to modulate gene expression, whereas a more specialized subset functions by binding directly to proteins (1). These include RNAs which contribute functions to ribonucleoprotein particles, such as the antiviral clustered, regularly interspaced, short palindromic repeats (CRISPR) locus RNAs (crRNAs) (2), and RNAs that antagonize the activity of proteins by sequestering them away from their substrates, such as CsrB (3) and the 6S RNA (4).

Toxin–antitoxin (TA) systems are nearly ubiquitous in prokaryotic genomes (5, 6), and small RNAs function as the antitoxin components in two of the five TA system types: type I antitoxins are small antisense RNAs that prevent translation of the toxin transcript, and type III antitoxins are small RNAs that inhibit their cognate protein toxins by direct interaction (7). Type II, type IV, and type V TA systems all use protein antitoxins with different mechanisms of action (7–9). Toxin targets are varied, although many act to degrade cellular RNAs. A canonical TA locus consists only of the genes for antitoxin and toxin arranged in a single operon. Toxins typically are more stable than antitoxins, so continued expression of the genes is required to maintain the antitoxin at protective levels; when the balance between the components is perturbed, the toxin is released and induces bacterial cell stasis or death. TA systems have been implicated in diverse cellular processes including plasmid stabilization, persistence, and resistance to viruses (10–12).

The prototype type III TA system is the plasmid-encoded ToxIN from *Pectobacterium atrosepticum* (hereafter $ToxIN_{Pa}$), which originally was discovered through its ability to confer bacteriophage resistance as an abortive infection system (12, 13). $ToxIN_{Pa}$ consists of a protein toxin ($ToxN_{Pa}$) and a small RNA antitoxin ($ToxI_{Pa}$), which have a kill/rescue phenotype when overexpressed in *Escherichia coli*. These elements occur genetically as a series of 5.5 tandem $toxI_{Pa}$ repeats followed by the $toxN_{Pa}$ gene. Both $toxI_{Pa}$ and $toxN_{Pa}$ are transcribed from the same promoter, and a transcriptional terminator between the two genes regulates the relative levels of toxin and antitoxin synthesis (Fig. 1*A*) (12). The purified complex of $ToxN_{Pa}$ and $ToxI_{Pa}$ cleaves housekeeping RNAs in vitro, suggesting that $ToxN_{Pa}$ is toxic in vivo by virtue of a general ribonuclease activity which is antagonized by the RNA antitoxin $ToxI_{Pa}$ (14). Bioinformatic searches subsequently identified numerous putative type III TA systems in diverse bacteria; these systems showed variation in their protein sequences and in the length, number, and sequence of their associated tandem repeats (12, 15). The toxin–antitoxin function of several of these systems was validated in *E. coli*, including that of plasmid-encoded ToxIN from *Bacillus thuringiensis* (hereafter $ToxIN_{Bt}$). The $toxIN_{Bt}$ locus comprises 2.9 $toxI_{Bt}$ antitoxic repeats together with the $toxN_{Bt}$ gene, which encodes a protein with 30% amino acid identity to $ToxN_{Pa}$.

$ToxI_{Pa}$ is a rare example of a naturally occurring small RNA which functions to counteract the activity of an enzyme. The crystal structure of $ToxN_{Pa}$ bound to $ToxI_{Pa}$ provided major insights into the mechanism of this antitoxic activity: three $ToxI_{Pa}$ RNAs, which are themselves cleaved from their repetitive precursor by $ToxN_{Pa}$, are bound head-to-tail by three $ToxN_{Pa}$ monomers to form a heterohexameric, triangular assembly in which the $ToxN_{Pa}$ active site is occluded (Fig. 1*A*) (14). Although illuminating, the structure of the $ToxIN_{Pa}$ complex naturally raised further questions about the system. First, how does $ToxN_{Pa}$, which has activity against a range of RNAs, recognize its $ToxI_{Pa}$ RNA antitoxin and assemble

Author contributions: F.L.S., X.Y.P., T.R.B., P.C.F., B.F.L., and G.P.C.S. designed research; F.L.S., X.Y.P., T.R.B., and S.-L.O. performed research; F.L.S., X.Y.P., T.R.B., S.-L.O., B.F.L., and G.P.C.S. analyzed data; F.L.S., X.Y.P., T.R.B., P.C.F., B.F.L., and G.P.C.S wrote the paper; and X.Y.P. solved the structure of the $ToxIN_{Bt}$ complex.

The authors declare no conflict of interest.

This article is a PNAS Direct Submission.

Data deposition: The crystallography, atomic coordinates, and structure factors reported in this paper have been deposited in the Protein Data Bank, www.pdb.org (PDB ID code 4ATO).

[1]Present address: Department of Molecular Cellular Biology, University of California, Berkeley, 360 Stanley Hall, Berkeley, CA 94720-3220.

[2]Present address: Department of Microbiology and Immunology, University of Otago, Dunedin 9054, New Zealand.

[3]To whom correspondence should be addressed. E-mail: gpcs2@cam.ac.uk.

See Author Summary on page 820 (volume 110, number 3).

This article contains supporting information online at www.pnas.org/lookup/suppl/doi:10.1073/pnas.1216039110/-/DCSupplemental.

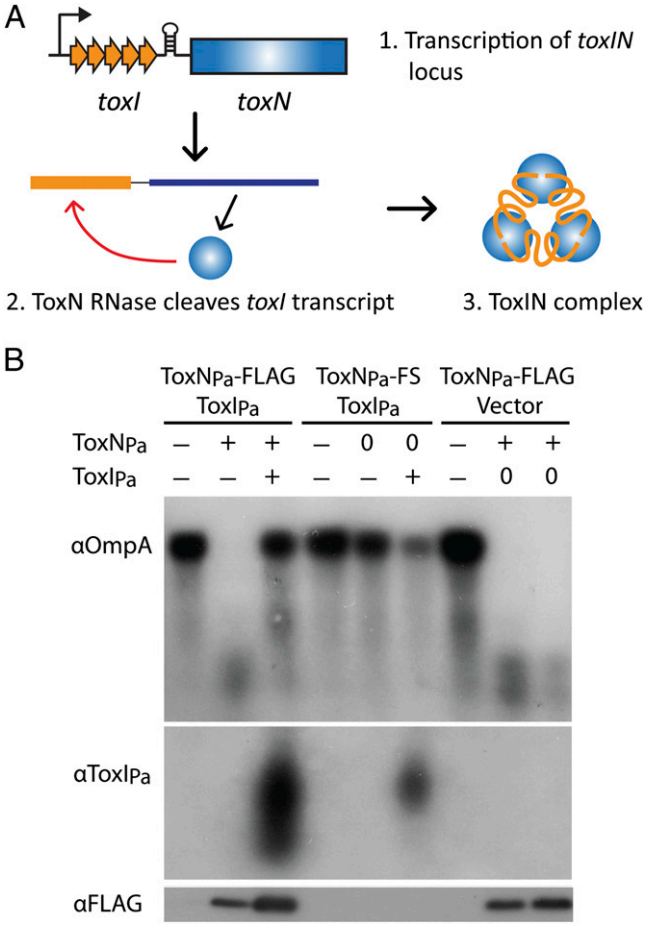


**Fig. 1.** $ToxN_{Pa}$ degrades RNAs and is inhibited by $ToxI_{Pa}$ in vivo. (*A*) Schematic representation of $ToxIN_{Pa}$ with $toxIN_{Pa}$ genetic organization, processing of $ToxI_{Pa}$, and complex formation indicated. $ToxN_{Pa}$ is shown in blue and $ToxI_{Pa}$ in orange. (*B*) $ToxN_{Pa}$ degrades the *ompA* transcript and is inhibited by $ToxI_{Pa}$ in vivo. *E. coli* cells containing separately inducible $ToxN_{Pa}$-FLAG and $ToxI_{Pa}$ plasmids were grown to log phase, and the effect of $ToxN_{Pa}$ expression and subsequent coexpression of $ToxI_{Pa}$ on *ompA* transcript levels was analyzed by Northern blot (*Top*). Expression of $ToxI_{Pa}$ (*Middle*) and $ToxN_{Pa}$-FLAG (*Bottom*) also was assessed by Northern and Western blot, respectively. The symbols "+" and "−" represent induction and repression of $ToxN_{Pa}$ or $ToxI_{Pa}$ expression. Induction of a negative control is indicated by "0." Because the RNA purification method used here excludes small RNAs, it was not possible to detect individual $ToxI_{Pa}$ repeats. Note that because $ToxN_{Pa}$-FS expression did not affect growth, cells reached stationary phase and showed natural down-regulation of *ompA* transcription over the course of the experiment.

into the triangular $ToxIN_{Pa}$ complex? Second, how do the processes of $ToxI_{Pa}$ cleavage and complex assembly relate to the inhibition of $ToxN_{Pa}$?

Here we demonstrate through cross-inhibition experiments with $ToxIN_{Bt}$ that ToxI RNA antitoxins are selective inhibitors of specific toxin partners. Both ToxIN systems have an "addictive" plasmid-maintenance phenotype. Specific inhibition of $ToxN_{Pa}$ ribonuclease can be mediated by both the processed and precursor forms of $ToxI_{Pa}$ in vitro and is linked to the self-assembly of the heterohexameric $ToxIN_{Pa}$ complex—a spontaneous process which occurs without requirement for exogenous energy or chaperones. We explain the basis for toxin–antitoxin specificity based on our crystal structure of the $ToxIN_{Bt}$ complex. Finally, we define the sequence-specific ribonuclease activity responsible for toxicity and antitoxin processing of two ToxN proteins.

## Results

**$ToxN_{Pa}$ Is a General Ribonuclease That Is Inhibited by $ToxI_{Pa}$ in Vivo.** We first tested the general ribonuclease activity of $ToxN_{Pa}$. Previous results suggested a general mRNA interferase function for $ToxN_{Pa}$; however, this activity was not shown directly, and $ToxN_{Pa}$ cleaved housekeeping gene transcripts in vitro even though it was present in complex with its antitoxin (14). In contrast, studies of mRNA interferases from type II TA systems showed that the addition of the antitoxin in a 1:1 stoichiometry completely inhibits the toxin's activity in vitro (16–18). To confirm the mechanism of $ToxN_{Pa}$ toxicity, Northern blots of the highly expressed housekeeping genes *ompA*, *dksA*, and *lpp* were performed following overexpression of $ToxN_{Pa}$ and the subsequent co-overexpression of $ToxI_{Pa}$. As shown in Fig. 1*B*, $ToxN_{Pa}$ overexpression caused a sharp reduction in the level of the *ompA* transcript, and subsequent overexpression of $ToxI_{Pa}$ restored *ompA* transcript levels. The degradation was not seen when an inactive, frameshifted $ToxN_{Pa}$ variant, ($ToxN_{Pa}$-FS) (12), was expressed, and *ompA* RNA levels were not restored in the $ToxI_{Pa}$ vector-only control strain. The same pattern of $ToxN_{Pa}$-mediated RNA degradation and $ToxI_{Pa}$-mediated rescue was seen with the *dksA* and *lpp* RNAs (Fig. S1). Overexpression of $ToxN_{Pa}$ also produced a broad size distribution of $ToxI_{Pa}$ products, showing that $ToxI_{Pa}$ is indeed processed by $ToxN_{Pa}$ in vivo. These results confirm the ribonuclease activity of $ToxN_{Pa}$ in vivo directed both to general cellular targets and to its own antitoxin transcript and the capacity of $ToxI_{Pa}$ to suppress this activity.

**ToxI Antitoxins Are Selective.** After confirming the ribonuclease activity of $ToxN_{Pa}$ in vivo and the action of $ToxI_{Pa}$ to neutralize this activity, we wished to explore the specificity of the ToxI RNA antitoxin. To do so, cross-inhibition experiments were performed with the $toxIN_{Pa}$ components and those of the related $toxIN_{Bt}$ system (Fig. 2*A*). Although the two ToxN proteins share 30% sequence identity, the corresponding cognate *toxI* RNA sequences are unrelated. In an *E. coli* kill/rescue assay, $ToxI_{Pa}$ counteracted $ToxN_{Pa}$ but not $ToxN_{Bt}$, and vice versa; each ToxI RNA antitoxin was active only against its own toxin partner (Fig. 2*B*). These experiments show that ToxI RNA antitoxins are highly selective inhibitors with the capacity to distinguish between closely related proteins.

**ToxIN Systems Promote Plasmid Maintenance.** Many TA systems can mediate plasmid stabilization by postsegregational killing, in which the rapid degradation of the antitoxin after plasmid loss results in the passive activation of the toxin to kill plasmid-

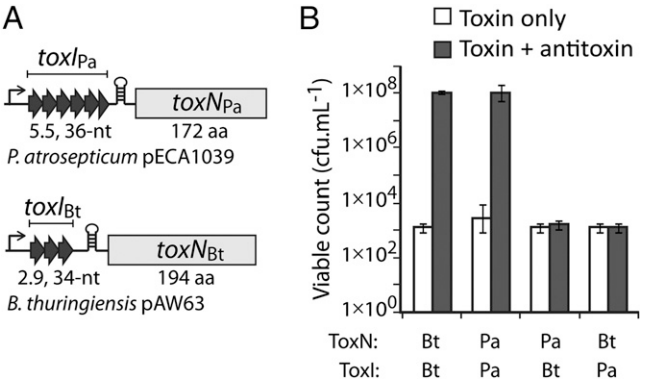


**Fig. 2.** ToxI antitoxins are selective for their cognate toxin. (*A*) Schematic of the $toxIN_{Pa}$ and $toxIN_{Bt}$ loci with the antitoxin and toxin components indicated. (*B*) Counts of viable *E. coli* DH5α following induction of $ToxN_{Bt}$ or $ToxN_{Pa}$ expression together with either $ToxI_{Bt}$ or $ToxI_{Pa}$. Results shown are mean and SD for three biological replicates.

free segregants (10). To determine whether $ToxIN_{Pa}$ and $ToxIN_{Bt}$ also have this activity, we performed long-term plasmid-loss experiments. $ToxIN_{Pa}$ completely prevented loss of plasmid pRBJ200 in *E. coli* W3110 over the duration of the experiment, whereas $ToxIN_{Bt}$ had no effect (Fig. 3*A*). However, $ToxIN_{Bt}$ did promote retention of the test plasmid pHCMC05 in *Bacillus subtilis* YB886 (Fig. 3*B*). Because the *Bacillus* test vector is based on the low-copy number pBS72 replicon (19), this stabilization activity is likely to apply to $ToxIN_{Bt}$ in its native context on *B. thuringiensis* plasmid pAW63 (20). This plasmid-stabilization function may represent the biological role of $ToxIN_{Bt}$, which, unlike $ToxIN_{Pa}$, did not have a detectable phage-resistance phenotype. The reason for the host dependence of this activity probably is that $ToxN_{Bt}$ is not toxic enough in *E. coli* to mediate postsegregational killing when expressed from its native promoter on a single-copy vector; $ToxN_{Bt}$ showed lower toxicity than $ToxN_{Pa}$ in *E. coli* (Fig. S2*A*). These results show that ToxIN systems are addictive modules that can enhance plasmid retention.

**$ToxN_{Pa}$ Is Inhibited by both Processed and Precursor $ToxI_{Pa}$.** In principle, toxin inhibition by ToxI RNA could require cleavage of the repetitive elements, for instance by linking the energy of cleavage with stable assembly. To test this possibility, stop-point RNA degradation assays were performed in vitro using purified $ToxN_{Pa}$ ribonuclease with *ompA* RNA as a substrate, and $ToxI_{Pa}$ RNA was added either as the long repetitive precursor, which was transcribed in vitro, or as precleaved, 36-nt pseudoknot repeats, which were purified from dissociated $ToxIN_{Pa}$ complex. $ToxN_{Pa}$ alone degraded the test substrate *ompA* to generate four major products (Fig. 4*A*, lanes 2–5), and addition of processed single repeats of $ToxI_{Pa}$ to the reaction in a 1:1 molar ratio of $ToxI_{Pa}$:$ToxN_{Pa}$ drastically reduced *ompA* degradation (Fig. 4*A*, lanes 6–8). Degradation of *ompA* RNA by $ToxN_{Pa}$ also was inhibited by addition of the long $ToxI_{Pa}$ precursor RNA, again in a 1:1 ratio of $ToxI_{Pa}$ repeats to $ToxN_{Pa}$ (each precursor RNA contains four copies of the functional $ToxI_{Pa}$ repeat). The precursor $ToxI_{Pa}$ was cleaved into progressively smaller units during the reaction and appeared to protect the *ompA* substrate from degradation completely (Fig. 4*A*, lanes 9–11), suggesting that the repetitive $ToxI_{Pa}$ RNA is a preferred substrate of $ToxN_{Pa}$. Addition of the $ToxI_{Bt}$ precursor did not prevent $ToxN_{Pa}$ cleavage of *ompA* (Fig. 4*A*, lanes 12–15), although the $ToxI_{Bt}$ RNA was cleaved by the toxin, further highlighting the selectivity of ToxI antitoxins observed in vivo. Within the resolution of this experiment, the repetitive $ToxI_{Pa}$ precursor appeared to be a more effective $ToxN_{Pa}$ inhibitor than its processed counterpart. These results indicate that the inhibitory action of the $ToxI_{Pa}$ RNA is entirely self-contained and occurs without cofactors or exogenous energy and that the energy of RNA cleavage is not necessary to form the inhibitory structure.

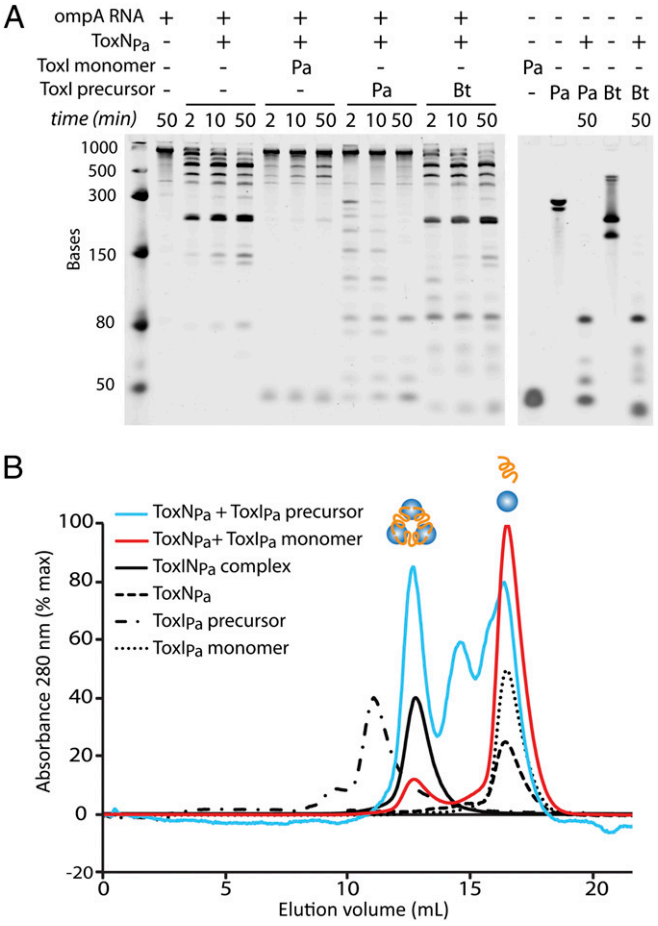


**Fig. 4.** $ToxI_{Pa}$ inhibits $ToxN_{Pa}$ and self-assembles the $ToxIN_{Pa}$ complex in vitro. (*A*) In vitro degradation of *ompA* RNA by $ToxN_{Pa}$ with different forms of added ToxI. Reactions (2 pmol *ompA* + 6 pmol $ToxN_{Pa}$) were incubated at 25 °C, and samples were taken at the times indicated. $ToxN_{Pa}$ protein and single $ToxI_{Pa}$ monomeric repeats were purified by FPLC. The full-length repetitive $ToxI_{Pa}$ and $ToxI_{Bt}$ precursor RNAs were transcribed in vitro. (*B*) Size-exclusion chromatography of $ToxIN_{Pa}$ assembled in vitro. $ToxN_{Pa}$ was incubated with $ToxI_{Pa}$ single repeats or full transcript for 1 h at 37 °C, and the reactions were analyzed by size-exclusion chromatography on an S200 13/30 column. Scaled absorbance traces are shown for $ToxN_{Pa}$ + single $ToxI_{Pa}$, $ToxN_{Pa}$ + full $ToxI_{Pa}$, $ToxIN_{Pa}$ complex, and each of the individual reaction components. The elution volume and calculated molecular weight of each peak are given in Table S1.

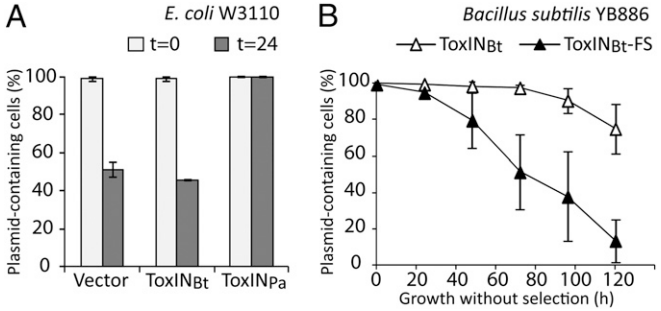


**Fig. 3.** ToxIN systems can stabilize plasmids. (*A*) Retention of $ToxIN_{Pa}$- and $ToxIN_{Bt}$-carrying plasmids in *E. coli* W3110. The percentage of cells retaining the plasmid before and 24 h after growth without selection is shown for $ToxIN_{Pa}$, $ToxIN_{Bt}$, and the vector-only control. (*B*) Retention of plasmids carrying $ToxIN_{Bt}$ or a frameshift $ToxIN_{Bt}$-FS negative control in *B. subtilis* YB886. The percentage of cells retaining the plasmid is plotted as a function of the number of hours of growth without selection. Both *A* and *B* show the mean and SD for three biological replicates.

Free $ToxI_{Pa}$ RNA is active as an inhibitor of $ToxN_{Pa}$, independently of its own cleavage. Free $ToxN_{Pa}$ also appeared to have higher activity than the purified $ToxIN_{Pa}$ complex in vitro (Fig. S2*B*). That $ToxI_{Pa}$ could inhibit $ToxN_{Pa}$ in vitro suggested that the heterohexameric $ToxIN_{Pa}$ complex may have assembled in these reactions; this possibility was examined next.

**$ToxIN_{Pa}$ Complex Can Self-Assemble in Vitro.** $ToxN_{Pa}$ was incubated with either processed $ToxI_{Pa}$ single repeats or with the in vitro transcribed $ToxI_{Pa}$ precursor, and the reactions were analyzed by size-exclusion chromatography (Fig. 4*B* and Table S1). Buffer conditions were kept the same as in the in vitro inhibition

experiment above. The $ToxN_{Pa}$ plus precursor $ToxI_{Pa}$ reaction eluted as three peaks, one at the same size as the $ToxIN_{Pa}$ complex, one at the elution volume of both $ToxN_{Pa}$ and $ToxI_{Pa}$, and an additional peak eluting at ~15 mL which contained the promoter and terminator sequences cleaved from either side of the $ToxI_{Pa}$ repeats in the long precursor RNA. The combination of $ToxN_{Pa}$ plus an overabundance of $ToxI_{Pa}$-processed single repeats gave a small peak of $ToxIN_{Pa}$ complex and a large peak of $ToxI_{Pa}$ monomer. All the detectable $ToxN_{Pa}$ in this reaction was contained in the complex peak. These results confirm that the $ToxIN_{Pa}$ complex can self-assemble in vitro from active $ToxN_{Pa}$ combined with either processed $ToxI_{Pa}$ or its long precursor RNA; the requirements for $ToxI_{Pa}$ cleavage, folding, and assembly into a stable complex are all intrinsic to the system. The inhibition of $ToxN_{Pa}$ by $ToxI_{Pa}$ observed in vitro therefore is linked to the spontaneous formation of the $ToxIN_{Pa}$ complex.

**Structure of $ToxIN_{Bt}$ Reveals the Basis for Antitoxin Specificity.** To understand better the selective inhibition displayed by ToxI antitoxins, we solved the structure of the $ToxIN_{Bt}$ complex to 2.2 Å by X-ray crystallography (see crystallographic statistics, Table S2). A modified $ToxN_{Pa}$ structure was used as the search model to obtain phase information by molecular replacement, and $ToxI_{Bt}$ RNA then was built into the omit map (Fig. S3*A*). Because the antitoxic repeats of *toxIN*$_{Bt}$ are not identical, the structure was solved and refined using the consensus $ToxI_{Bt}$ RNA repeat sequence, which is offset −8 nt relative to the genetic *toxI*$_{Bt}$ repeat (Fig. S3*B*). $ToxI_{Bt}$ nucleotides are numbered 1→34 based on the RNA observed in the structure.

$ToxIN_{Bt}$ is a heterohexameric, triangular assembly of three ToxN protomers and three ToxI RNAs (Fig. 5*A*), which is generated by a threefold rotational symmetry operation on the crystal asymmetric unit of $1ToxN_{Bt}$:$1ToxI_{Bt}$. The bound $ToxI_{Bt}$ units are cleavage products of $ToxN_{Bt}$, as shown by their pseudocontinuous arrangement and by the presence of a 2′-3′-cyclic phosphate at the 3′ end of each $ToxI_{Bt}$, which was observed in the omit map with density at a contour level >3 σ. The processing of ToxI by ToxN and the core architecture of the resulting complex are shared between $ToxIN_{Bt}$ and $ToxIN_{Pa}$.

The processed $ToxI_{Bt}$ RNA folds into a compact pseudoknot core, containing three internal base triplexes, with two single-stranded tails. This architecture creates two large surfaces for interaction with $ToxN_{Bt}$, each formed from one face of the pseudoknot core and one of the single-stranded tails (Fig. 5 *B* and *C*). Although *toxI*$_{Bt}$ did not have any detectable sequence similarity to *toxI*$_{Pa}$ a priori, the key structural features of the processed inhibitory $ToxI_{Bt}$ RNA, and the nucleotides involved, are conserved with $ToxI_{Pa}$ (Fig. S4). The two base-paired stems of the pseudoknot are separated by a single-tiered G:U:U base triplex (triplex 3, G23:U16:U24; see Fig. 7*A*), and these three elements stack in a quasi-continuous helical core, which is stabilized further by interdigitation of the G23 purine ring between U8 and U9 at the base of stem I. The precise tertiary structure of $ToxI_{Bt}$ is maintained by an extensive internal hydrogen-bonding network involving all but two nucleotides of the central pseudoknot. This network includes several noncanonical base pairs and backbone–base interactions in addition to the Watson–Crick pairs of the pseudoknot stems (Fig. 5*B*). The absolute conservation of both triplex 3 and the guanine base interdigitation between $ToxI_{Bt}$ and $ToxI_{Pa}$ suggests that these interactions are required for the formation or maintenance of the ToxI fold. Importantly, conservation of these core structural elements does not preclude changes to ToxN-interactive regions of ToxI, which could impart specificity to the ToxI–ToxN interaction.

The toxin protein $ToxN_{Bt}$ comprises a highly twisted, antiparallel β-sheet core flanked by several helices, including the long, kinked helix H3 (Fig. 6*A*), the same core fold as in $ToxN_{Pa}$. Both ToxN proteins are structural homologs of the MazF/Kid

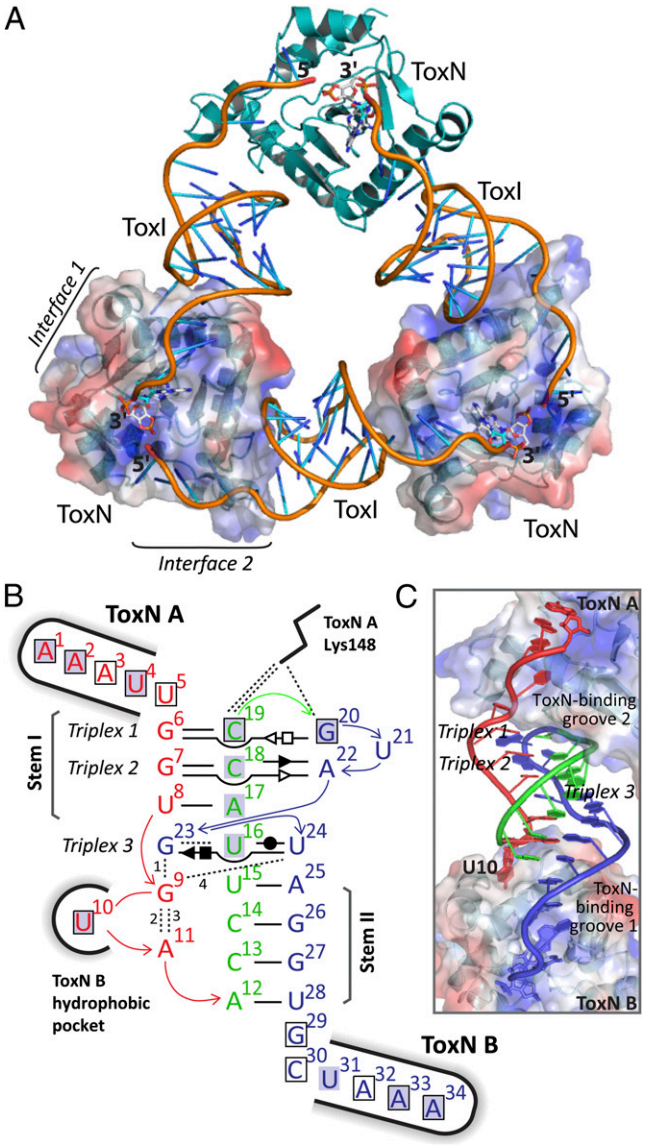


**Fig. 5.** Structure of the $ToxIN_{Bt}$ complex. (*A*) The trimeric $ToxIN_{Bt}$ complex. $ToxN_{Bt}$ is shown in cartoon representation in teal, and the $ToxI_{Bt}$ RNA backbone is orange with the bases colored in a gradient from orange to blue. The surface of two $ToxN_{Bt}$ monomers is shown also, with blue for positively charged and red for negatively charged regions. In each $ToxI_{Bt}$ protomer the nucleotide A34 and its 2′,3′-cyclic phosphate are shown as white sticks. (*B*) Schematic of internal and external bonding of a single $ToxI_{Bt}$ monomer. Canonical Watson–Crick A:T or G:C base pairs are represented by a single, black horizontal bar. Noncanonical base pairs of $ToxI_{Bt}$ are shown in Leontis–Westhof symbols (49) with the interacting edges indicated as follows: Watson–Crick edge, ●; sugar edge, ►; Hoogsteen edge, ■. Filled and open symbols indicate the *cis* or *trans* orientation of the glycosidic bonds, respectively. The vertically aligned letters indicate stacked bases. Black dashed lines indicate single hydrogen-bond interactions. Bonds numbered 1–4 involve backbone atoms as follows: 1, G9 (N3) to G23 (O2); 2, G9 (N7) to A11 (O2); 3, G9 (O2) to A11 (PO2); 4, G9 (N2) to U24 (PO2). The $ToxN_{Bt}$ monomers at key interaction sites are indicated, and interactions between $ToxI_{Bt}$ nucleotides and $ToxN_{Bt}$ are indicated with a black outline to show base–$ToxN_{Bt}$ interactions or a gray highlight to indicate backbone–$ToxN_{Bt}$ interactions. See Fig. S4 for comparison with the $ToxI_{Pa}$ structure. (*C*) A single $ToxI_{Bt}$ pseudoknot, bound by two monomers of $ToxN_{Bt}$ (labeled '"A" and "B"). $ToxI_{Bt}$ is shown as a cartoon with nucleotides colored according to their location as in panel *B*. $ToxN_{Bt}$ monomers are shown as a cartoon beneath a surface representation with positively and negatively charged regions colored in blue and red, respectively.

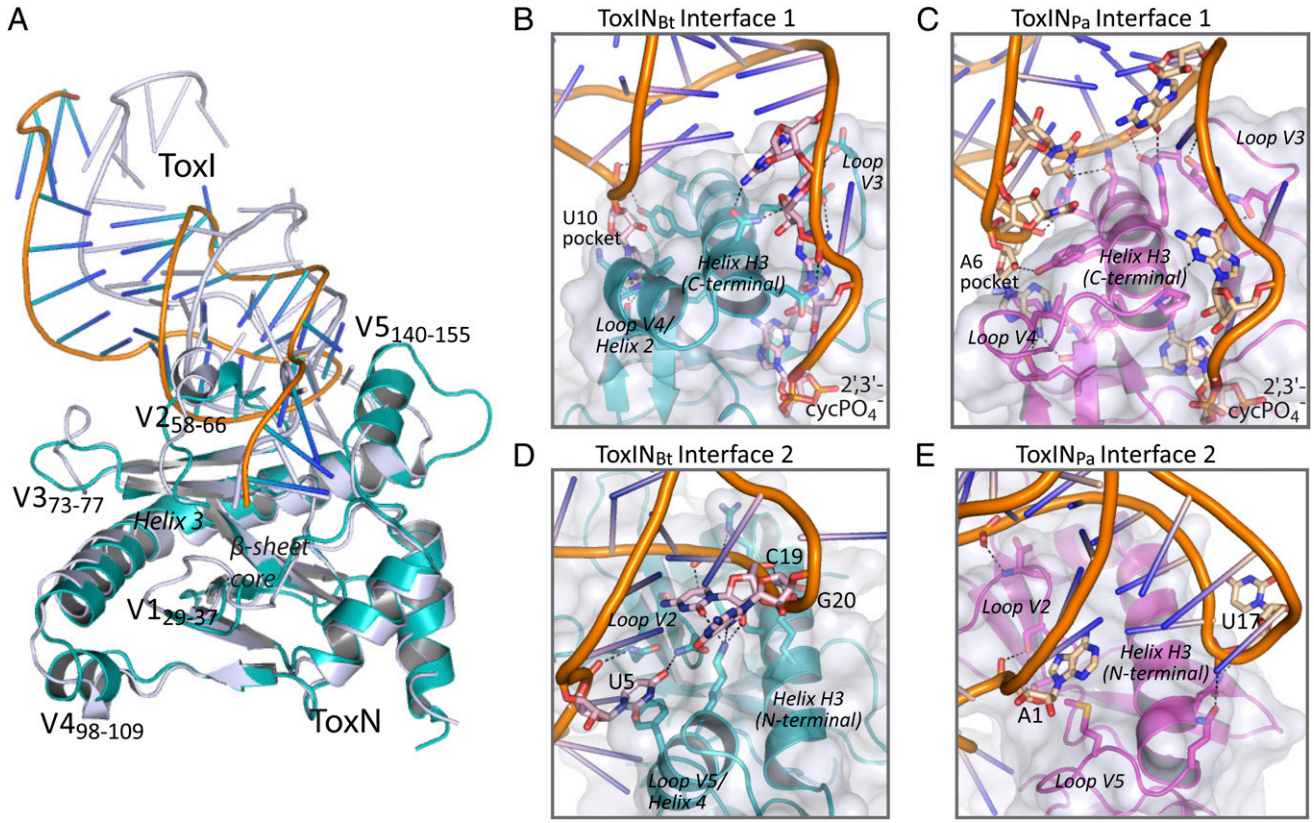


**Fig. 6.** $ToxIN_{Bt}$ and $ToxIN_{Pa}$ have different protein–RNA interfaces. (*A*) Least-squares superimposition of the *B. thuringiensis* $ToxN_{Bt}$ and *P. atrosepticum* $ToxN_{Pa}$ (PDB ID code 2XD0) protein structures. The superimposed protein monomers are each shown with one associated ToxI RNA pseudoknot (corresponding to interface 2). $ToxN_{Bt}$ is shown in teal, $ToxI_{Bt}$ is shown in orange and blue, and both $ToxN_{Pa}$ and $ToxI_{Pa}$ are shown in silver. Variable loop regions are labeled V1–V5 and are numbered according to the corresponding residues of $ToxN_{Bt}$. (*B–E*) Comparison of ToxI–ToxN interfaces in the $ToxIN_{Bt}$ and $ToxIN_{Pa}$ complex structures. ToxI RNAs are shown as cartoons with key nucleotides represented as sticks in pale pink ($ToxI_{Bt}$) or pale yellow ($ToxI_{Pa}$). ToxN proteins are shown as cartoons in teal ($ToxN_{Bt}$) or magenta ($ToxN_{Pa}$) with key residues represented as sticks. Structural regions of ToxN are indicated. Black dashed lines indicate hydrogen bonds of 2.6–3.4 Å.

family of type II TA system toxins, with additional features to facilitate binding to ToxI (21). However, an overlay of the two protein structures does show five key variable regions (V1–V5) (Fig. 6*A*): the $ToxN_{Bt}$ active site loop S1→S2 (V1; residues F29 R37); loop S3→S4 (V2; R58–Q66), which is α-helical in $ToxN_{Pa}$ but a short $3_{10}$ helix in $ToxN_{Bt}$; loop S4→S5 (V3; D73–K77); and helices H2 and H4 (V4 and V5; residues I98–Q109 and T140–V155, respectively), which are insertions in $ToxN_{Pa}$ S7→H3 and H3→H5, respectively. Strikingly, these five variable regions are the main sites for interaction of the protein with ToxI. A protein sequence alignment of $ToxN_{Bt}$ and $ToxN_{Pa}$ with six additional ToxN-family proteins also shows a largely conserved secondary structure, with the variability between homologs clustered in these five loop regions (Fig. S5). It appears that the same core fold is shared across the entire ToxN family, but each protein has a unique set of variable loops reflecting the different antitoxin specificity of each member of the ToxN family.

Two extended interfaces sustain the trimeric $ToxIN_{Bt}$ assembly, each formed from a section of the kinked helix H3 and two variable surface loops of $ToxN_{Bt}$ interacting with one binding groove of $ToxI_{Bt}$. Interface 1, where $ToxI_{Bt}$ groove 1 interacts with the N-terminal portion of H3 (Fig. 6*B*), is maintained by U10 binding in a hydrophobic pocket formed by the $ToxN_{Bt}$ loop V4 and helix H3 and the binding of the single-stranded $ToxI_{Bt}$ tail across the surface groove of $ToxN_{Bt}$. This interface, which buries ∼1,000 Å$^2$, involves far fewer interactions than interface 1 of $ToxIN_{Pa}$ (Fig. 6*C*). At $ToxIN_{Bt}$ interface 2, the RNA chain of $ToxI_{Bt}$ groove 2 wraps around the surface of $ToxN_{Bt}$ at loop V2 and across helix H3 (Fig. 6*D*). The RNA is positioned by base-specific hydrogen bonding and hydrophobic interactions between sidechains of loops V2 and V5 and bases C19 and U5 and by an extended series of hydrogen bonds between the positively charged side chains along helix H3 and the phosphate backbone of $ToxI_{Bt}$ G20–A17 (Fig. 6*D* and Fig. S4*C*). This interface also differs notably from its equivalent in $ToxIN_{Pa}$ (Fig. 6*E*), because a shortening of the $ToxI_{Bt}$ groove 2 loop together with a nine-residue insertion in $ToxN_{Bt}$ loop V5 allows the two components to pack more closely. The buried surface area of interface 2 is ∼1,180 Å$^2$. An effect of the changes to the interface interactions in $ToxIN_{Bt}$ is that each $ToxI_{Bt}$ unit leaves its bound $ToxN_{Bt}$ monomer at a different angle than in $ToxI_{Pa}$, so the central axis of each $ToxI_{Bt}$ pseudoknot deviates further from the triangular frame of the three $ToxN_{Bt}$ monomers, although the overall triangular complex architecture is retained (Figs. 5*A* and 6*A*).

In summary, both $ToxI_{Bt}$ and $ToxN_{Bt}$ have structures similar to their *P. atrosepticum* equivalents, but subtle, complementary changes to both toxin and antitoxin result in substantial differences in the protein–RNA interfaces that maintain the inactive complex.

**$ToxI_{Bt}$ Contains a Rare C:G:G *cis* Watson–Watson/*trans* Sugar–Hoogsteen Triplex.** The three base triplexes of $ToxI_{Bt}$ are shown in Fig. 7*A* along with their geometric classification (22). Triplex 1 is a notable point of difference between $ToxI_{Pa}$ and $ToxI_{Bt}$: In $ToxI_{Pa}$ triplex 1 is a type II A-minor motif of the stem I base pair G2:C15 with A19 of the following loop. In $ToxI_{Bt}$ triplex 1 the loop following the stem I base pair G6:C19 is absent. Instead, the adjacent nucleotide

G20 interacts with the minor-groove edge of the base pair via its Hoogsteen face to form a rare C:G:G cWW/tSH *cis* Watson–Watson/*trans* Sugar–Hoogsteen (cWW/tSH) triplex, which has been observed only once before, in the *E. coli* 16S rRNA (22, 23). Triplexes 2 and 3 are conserved between $ToxI_{Bt}$ and $ToxI_{Pa}$, and both are common RNA tertiary motifs. Triplex 2 is a type I A-minor motif (24) formed from the stem 1 base pair G7:C18 with A22, whereas Triplex 3 comprises the U24:U16 pair, with G23 interacting with the major groove edge of this pair (Fig. 7*A*).

$ToxI_{Bt}$ Triplex 1 is stabilized by hydrogen bonds from Lys148 of $ToxN_{Bt}$ to C19 and G20. Because Lys148 is not conserved in other ToxN homologs (Fig. S5), this interaction may be unique to $ToxIN_{Bt}$. The importance of interaction with Lys148 for antitoxicity could not be assessed, because mutation of Lys148 to alanine abolished toxicity (Fig. 7*C*). Mutation of G20 had only a minimal effect on antitoxicity, suggesting other nucleotides can form a functional platform in this position (Fig. 7*B*). Specific mutations to other $ToxI_{Bt}$ nucleotides confirmed the importance of the intercalated base G23, its stacking partners U8 and G9, and the $ToxN_{Bt}$-binding U10, with these mutants showing reduced activity in a kill/rescue assay with $ToxN_{Bt}$ (Fig. 7*B*).

**$ToxN_{Pa}$ and $ToxN_{Bt}$ Are Sequence-Specific Endoribonucleases with Different Substrate Preferences.** $ToxN_{Pa}$ and $ToxN_{Bt}$ are both bacteriostatic ribonucleases that cleave their own antitoxins. $ToxN_{Bt}$ has a ribonuclease active site similar to that of $ToxN_{Pa}$ (Fig. 8 *A* and *B*). The 2′-3′-cyclic phosphate product is held by an extensive hydrogen-bond network formed from the basic residues Lys31, Arg37, and Arg58 and the conserved Ser57 and Thr56 close to the 2′O of the cyclic phosphate. The purine ring of A34 is coordinated in the *anti*- conformation by Tyr110 and Gln117, as in $ToxIN_{Pa}$. Several of the active-site residues were shown by mutagenesis to be required for toxicity (Fig. 7*C*). ToxN enzymes are proposed to cleave their substrates through a metal-independent RNase T1-like mechanism, based on their active-site architectures, the presence of the 2′-3′-cyclic phosphate product in the active site, and their structural homology to Kid, whose reaction mechanism has been studied in detail (21, 25). The RNA fragment patterns produced by $ToxN_{Pa}$ degradation in vitro (Fig. 8*C* and ref. 14), together with the precise ToxI–ToxN interactions observed in both complex structures, suggested sequence-specific ribonuclease activity. Both $ToxIN_{Pa}$ and $ToxIN_{Bt}$ cleaved several highly expressed *E. coli* test substrates—*rpoD*, *ompF*, *ompA* and *dksA*—into defined patterns of RNA fragments in vitro (Fig. 8*C*). Sites of ToxN-mediated cleavage then were identified by performing 5′ RACE on the cleaved RNA substrates, and sequence-specificity profiles were generated from a total of 14 unique 5′ fragment ends for $ToxIN_{Pa}$ and 12 unique ends for $ToxIN_{Bt}$. $ToxN_{Pa}$ cleaves RNAs at AA↓AU sequences, and in two instances, at AA↓AG (Fig. 8*D*). $ToxN_{Bt}$ recognizes the sequence A↓AAAA with some tolerance for different nucleotides at positions +2 and +4 (Fig. 8*D*). The in vitro sequence specificity matches the active-site interactions seen in both ToxIN complexes; in $ToxIN_{Bt}$ A34 is specifically coordinated; the purine rings of A1→A3 bases form a hydrophobic stack supported by Phe29, which is required for toxicity; and A1 and A3 also make base-specific hydrogen bonds to $ToxN_{Bt}$ (Fig. 8*A*). In $ToxN_{Pa}$ all three adenines of the AA↓AU sequence are held by specific hydrogen bonds to the protein, whereas the U pyrimidine ring stacks between A3 and Phe88 (Fig. 8*B*). Therefore both ToxN ribonucleases have sequence-specific activity consistent with a general mRNA interferase mechanism of toxicity. Unlike the ribonuclease toxins of type II TA systems, this activity also is required to generate the mature antitoxin.

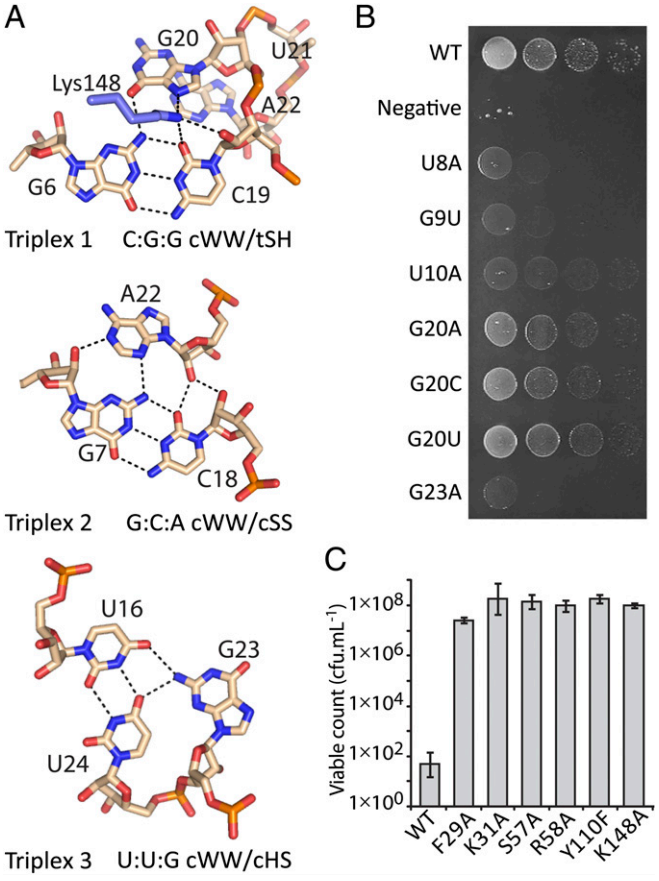


**Fig. 7.** $ToxI_{Bt}$ triplex structures and $ToxIN_{Bt}$ mutagenesis study. (*A*) Details of the three base triplexes of $ToxI_{Bt}$, shown as pale pink sticks with black dashed lines to indicate hydrogen bonds. Lys148 of $ToxN_{Bt}$ is shown in blue. The geometric classification of each triplex is indicated (22). (*B*) Analysis of effects of $ToxI_{Bt}$ mutations in vivo. Growth of *E. coli* DH5α following co-overexpression of $ToxN_{Bt}$ with mutants of $ToxI_{Bt}$ is shown and is representative of three biological replicates. (*C*) Effect of $ToxN_{Bt}$ mutations in vivo. Viable counts of *E. coli* cells overexpressing $ToxN_{Bt}$ mutant constructs are shown as mean ± SD.

## Discussion

The potential for small RNAs to act as protein agonists has long been appreciated, as demonstrated by the directed evolution of RNA aptamers that inhibit HIV reverse transcriptase (26) and influenza virus B hemagglutinin (27), among others (28). Despite the successful experimental generation of these artificial species, there are very few examples of naturally occurring RNAs that act directly to impede protein activity in vivo, and ToxI antitoxins are, to our knowledge, the only RNAs whose function is to inhibit their own parent-processing enzyme. The questions naturally arise as to how they work and what is the origin of their molecular specificity. We show that ToxI antitoxins are selective enzyme inhibitors and that the capacities to inhibit the protein and to assemble the $ToxIN_{Pa}$ complex are determined entirely by the sequence of the $ToxI_{Pa}$ RNA and its interactions with its cognate toxin. We also show that ToxIN systems, in addition to their role in phage resistance (12, 13), have an addictive plasmid-maintenance activity, which likely contributes to their evolutionary success. The structural basis for ToxI antitoxin specificity is revealed through the crystal structure of a second ToxIN system. Finally, we show that ToxN proteins have a sequence-specific ribonuclease activity responsible both for their toxicity and for processing of their own RNA inhibitors.

$ToxI_{Pa}$ inhibited $ToxN_{Pa}$ in vitro, in both its processed and precursor forms (Fig. 4*A*), and the $ToxI_{Pa}$ precursor also appeared to act as a preferred $ToxN_{Pa}$ substrate. Therefore the requirements for toxin inhibition are contained entirely in the sequence of the repetitive $ToxI_{Pa}$ transcript and are retained after cleavage into single pseudoknot units. Whether folding of the $ToxI_{Pa}$

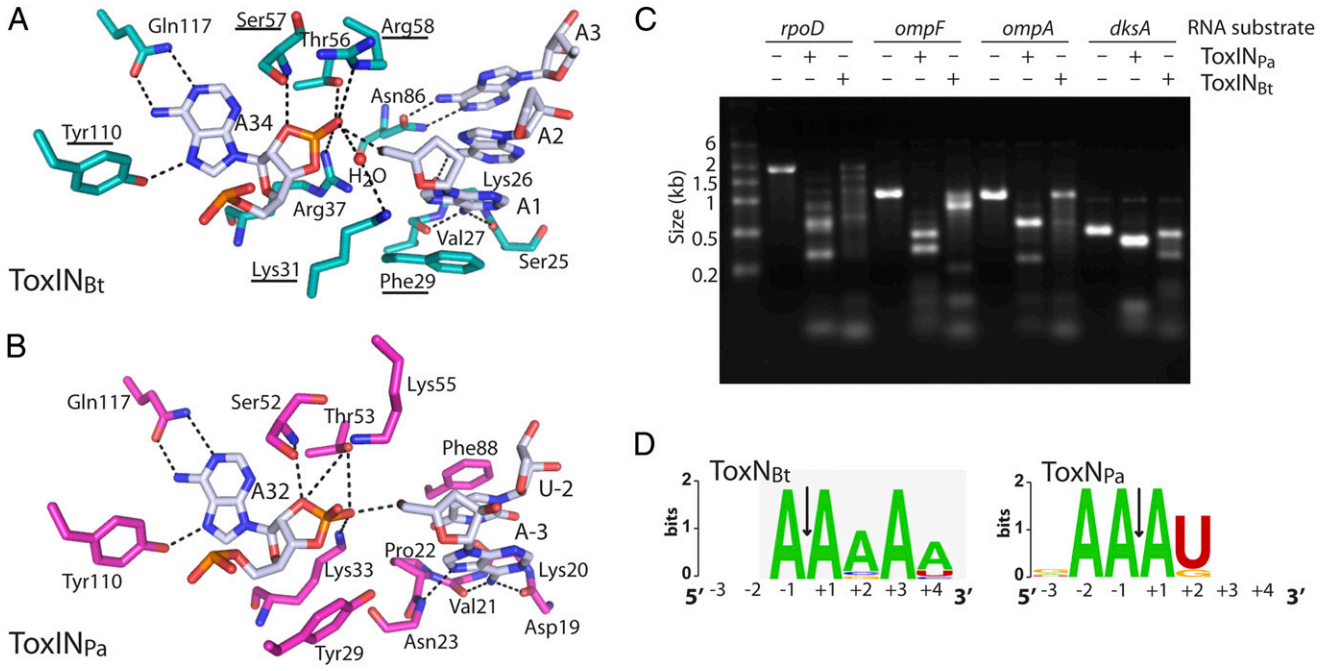


**Fig. 8.** $ToxN_{Bt}$ and $ToxN_{Pa}$ are endoribonucleases with selective substrate preferences. (*A*) View of $ToxIN_{Bt}$ active site showing key interactions for product recognition and substrate cleavage. $ToxN_{Bt}$ is shown in teal and $ToxI_{Bt}$ RNA in white. Hydrogen bonds are indicated by black dashed lines. Residues that were mutated resulting in a loss of toxicity are underlined (see also Fig. 7*C*). Phosphate groups of the $ToxI_{Bt}$ backbone are omitted for clarity. (*B*) Active site of $ToxIN_{Pa}$ (PDB ID 2XDB). $ToxN_{Pa}$ is shown in light magenta and $ToxI_{Pa}$ in white. (*C*) In vitro degradation products of $ToxIN_{Pa}$ and $ToxIN_{Bt}$. Substrate RNAs were incubated with purified ToxIN complex at a 1:4 molar ratio, and the products were examined by agarose gel electrophoresis. (*D*) Sequence-preference profiles of $ToxN_{Bt}$ and $ToxN_{Pa}$, generated by performing 5′ RACE on the $ToxIN_{Bt}$- and $ToxIN_{Pa}$-cleavage products of *E. coli rpoD*, *ompF*, *ompA*, and *dksA* RNAs. The sequence-preference profiles shown are from a total of 14 ($ToxIN_{Pa}$) and 12 ($ToxIN_{Bt}$) unique 5′ ends.

pseudoknot occurs before or concomitantly with binding and cleavage by $ToxN_{Pa}$ remains to be addressed experimentally. The $ToxIN_{Pa}$ complex assembled spontaneously when its components were combined in vitro, suggesting that toxin inhibition and formation of the trimeric protein–RNA complex are inextricably linked. Our results in vitro indicate that $ToxI_{Pa}$ RNA is likely to be an extremely efficient and potent inhibitor of $ToxN_{Pa}$ in vivo: Formation of the inhibited $ToxIN_{Pa}$ complex is robust, and the $ToxI_{Pa}$ precursor diverts free $ToxN_{Pa}$ away from other substrates. Furthermore, these cleavage and inhibition events in vivo would occur in the context of a constant oversupply of $ToxI_{Pa}$ precursor (12). The use of an RNA (rather than a protein) inhibitor in type III TA systems may offer benefits to the cell, such as a reduced metabolic cost and increased sensitivity to global changes in rates of protein and RNA synthesis. Our results suggest that these benefits do not come at a cost of reduced protection by the antitoxin.

The $ToxI_{Bt}$ and $ToxI_{Pa}$ RNAs are both pseudoknots (Fig. 5 *B* and *C* and Fig. S4), and this fold is likely to be conserved across the ToxI family despite considerable variation in primary sequence (15). Pseudoknot folds are a dominant form for structured RNAs, because this architecture is generally compact but can create accommodating surfaces for interaction with other molecules (29, 30). As a result, pseudoknot folds have been identified in functionally diverse RNAs including ribozymes (31), riboswitches (32, 33), and several RNA aptamers (26, 34). ToxI antitoxins are natural examples of RNA pseudoknots that inhibit enzymes, mirroring a function originally observed in artificially generated aptamers.

ToxI-mediated inhibition is selective (Fig. 2*B*), and the crystal structure of a second ToxIN system showed how this specificity is achieved. The $ToxI_{Bt}$ and $ToxN_{Bt}$ components are broadly similar to their *Pectobacterium* orthologs. However, minor changes in these components lead to substantial changes in the two extended protein–RNA interfaces of the ToxIN complex. Within the framework of a 3ToxI:3ToxN triangular complex, antitoxin binding appears to be specific and mediated primarily by a few variable regions of a common ToxN scaffold (Fig. 6 *A*–*E*). In addition, the mature form of each ToxI is generated through the sequence-specific RNase activity of its cognate toxin. Note that although $ToxN_{Pa}$ cleaved the $ToxI_{Bt}$ precursor in vitro (Fig. 4*A*), cleavage at each AA↓AU sequence would not generate the same 34-nt inhibitory units observed in the $ToxIN_{Bt}$ complex (see Fig. S3*B*). In summary, $ToxN_{Bt}$ and $ToxN_{Pa}$ differ in both structure and endoribonuclease specificity, and these differences are matched by variations in their cognate antitoxins. These differences reflect the coevolution of each toxin with its inhibitory RNA partner and the selective pressure to maintain processing of the antitoxic RNA and formation of a stable complex.

The biological function of ToxI antitoxins to inhibit their own parent-processing enzymes is, to our knowledge, unique. However, parallels can be drawn between ToxN proteins and type I Cas6 ribonucleases of the anti-viral CRISPR/Cas systems, which also remain bound to their own catalytic product following cleavage of their CRISPR transcript substrates into crRNAs (35, 36). However, the functional consequences of these events are different. ToxI RNAs inhibit their processing enzymes to protect the cell from a harmful general RNase, whereas binding of crRNAs to their Cas6-processing enzymes (which do not cleave other RNAs) leads to formation of the Cascade ribonucleoprotein complex and its highly specific recognition of invading nucleic acids.

$ToxN_{Bt}$ and $ToxN_{Pa}$ displayed sequence-specific ribonuclease activity (Fig. 8), which also has been observed for numerous type II toxins including MazF and Kid (16, 17). Although there are examples of TA system toxins that target specific RNAs in vivo, including several VapC and MazF homologs (37–39), our Northern blot results show that $ToxN_{Pa}$ is unlikely to do so, because this enzyme degraded all three transcripts tested (Fig. 1*B* and Fig. S1). This general RNase mechanism of toxicity is assumed

to be the same for $ToxN_{Bt}$, which has a longer recognition sequence but greater tolerance for variations.

$ToxIN_{Pa}$ is a powerful antiviral abortive infection system which also can stabilize plasmids (Fig. 2*A* and refs. 12 and 13). $ToxIN_{Bt}$ can stabilize plasmids in a *Bacillus* host (Fig. 2*B*), but, unexpectedly, did not affect the replication of any of >100 environmental *Bacillus* phages. Therefore $ToxIN_{Bt}$ likely functions in vivo to promote the maintenance of plasmid pAW63, although additional functions are possible. Type III TA systems are found in the chromosomes and plasmids of multiple prokaryotic phyla and appear to be horizontally transferred throughout these genomes (15). The broad-ranging ribonuclease specificity of the two ToxN homologs, and the demonstration of toxin inhibition and complex assembly in vitro, suggest that toxicity and antitoxicity have very little dependence on the host and so could be maintained even when these loci are transferred to distantly related bacteria. Indeed, the structurally similar $ToxIN_{Pa}$ and $ToxIN_{Bt}$ are both functional and able to confer adaptive benefits in their very distantly related Enterobacterium and Firmicute hosts. Our research presents a scenario in which ToxIN is an entirely self-contained, addictive, and potentially lethal molecular machine upon which evolution can act to drive distinct adaptive advantages within different populations of bacterial hosts.

## Materials and Methods

**Northern Blot.** *E. coli* DH5α strains carrying the plasmid pairs pTRB1/pTA76, pTA50/pTA76, or pTRB1/pTA100 (Table S3) were grown in 25 mL LB plus 0.2% (wt/vol) glucose as shaking cultures at 37 °C to $OD_{600}$ 0.6–0.8. Cells were spun down, resuspended in 25 mL LB plus 0.1% (wt/vol) L-arabinose to induce expression of $ToxN_{Pa}$, and grown at 37 °C for a further 2 h. $ToxI_{Pa}$ expression then was induced by addition of 1 mM isopropylthio-β-galactoside (IPTG), and cells were grown for a further 4 h. RNA was extracted from cell samples before and after $ToxN_{Pa}$ expression and after coexpression of $ToxI_{Pa}$, using an RNeasy kit (Qiagen). Antisense 3′-digoxigenin (DIG)–labeled RNA probes were transcribed in vitro from PCR products [αOmpA: pFLS50, primers FS61/TRB230; αToxI–pTA110: primers M13-20/TRB57 (Tables S3 and S4)] and used for Northern blotting of 3.5 μg total RNA according to the DIG user manual (Roche). Cell samples taken before and after $ToxN_{Pa}$ expression and after coexpression of $ToxI_{Pa}$ also were analyzed by Western blot for the FLAG-tagged $ToxN_{Pa}$ protein, as reported previously (12).

**$ToxIN_{Bt}$ Mutagenesis and Toxicity/Antitoxicity Assays.** $ToxN_{Bt}$ mutants were constructed by overlap-extension PCR and were cloned into pBAD30 (40). Single-repeat $ToxI_{Bt}$ sequences were cloned into pTA100 as described (12). Single strains of *E. coli* DH5α were cotransformed with one $ToxN_{Bt}$ and one $ToxI_{Bt}$ plasmid (Table S3) and were used for overexpression-based toxicity and antitoxicity assays as described (12).$ToxIN_{Bt}$–$ToxIN_{Pa}$ cross-talk experiments were performed in the same way, using pTA100-derived ToxI constructs containing the full series of repeats and pBAD30-derived ToxN constructs (Table S3).

**Plasmid-Loss Assays.** Plasmid-loss experiments were performed in *B. subtilis* YB886 with plasmids pFLS79 and pFLS80 and in *E. coli* W3110 with plasmids pFLS118 and pFLS121 and the pRBJ200 vector control (Table S3). *B. subtilis* YB886 cells carrying test plasmids were grown overnight in LB supplemented with 10 $\mu g \cdot mL^{-1}$ chloramphenicol. Fresh LB medium without antibiotics was inoculated with overnight culture at a calculated $OD_{600}$ of $5 \times 10^{-7}$, and the culture was grown at 28 °C. Cultures were reinoculated into fresh LB at a starting $OD_{600}$ of $5 \times 10^{-7}$ every 24 h to maintain exponential growth. The proportion of plasmid-containing cells at each time point was determined by serially diluting the cultures and plating on LB agar, then patching colonies onto LB plates supplemented with 10 $\mu g \cdot mL^{-1}$ chloramphenicol. Plasmid-loss experiments using *E. coli* W3110 were performed as described previously (41) with nonselective exponential growth maintained for 24 h.

**Purification of $ToxN_{Pa}$, $ToxI_{Pa}$ and $ToxIN_{Pa}$.** $ToxIN_{Pa}$ was expressed and purified from *E. coli* ER2566 pTRB14/pTRB18 as reported previously (14). A small proportion of the $ToxIN_{Pa}$ complex dissociated between the affinity and anion exchange purification steps, so separate fractions of $ToxN_{Pa}$ and $ToxI_{Pa}$ were isolated by anion exchange chromatography in the same purification run as the trimeric $ToxIN_{Pa}$ complex. Samples were concentrated and exchanged into gel filtration buffer (150 mM NaCl, 50 mM Tris·HCl, 1 mM DTT, pH 7.5) before use in RNA-degradation or complex-reassembly experiments.

**In Vitro RNA Degradation Assays.** The full $ToxI_{Pa}$ and $ToxI_{Bt}$ precursor RNAs were transcribed in vitro from PCR products generated using the template/primer combinations pTA111:M13-20/MJ12 and pFLS66:M13-20/PF196 (Tables S3 and S4). $ToxN_{Pa}$ protein and $ToxI_{Pa}$ single repeats were purified by FPLC. RNA degradation reactions of 15-μL volume were set up in assay buffer [150 mM NaCl, 50 mM Tris·HCl (pH 7.5)] with *E. coli ompA* RNA (700 ng or 2 pmol) and $ToxN_{Pa}$ in a 1:3 molar ratio, and ToxI RNA added at a 1:1 molar ratio of ToxI repeats to $ToxN_{Pa}$ monomers. $ToxN_{Pa}$ and ToxI components were allowed to react at 25 °C for 2 min before reactions were started by the addition of the *ompA* substrate. Time-point samples of 5 μL each were quenched in 5 μL 2× RNA loading buffer (Fermentas) and flash-frozen in liquid nitrogen. Reaction products were visualized by electrophoresis on a 6% (wt/vol) acrylamide TBE-Urea gel (UreaGel, National Diagnostics) followed by staining with SYBR Gold (Invitrogen).

**$ToxIN_{Pa}$ Complex Reassembly Reactions and Gel Filtration.** Reassembly reaction 1 contained 10 μg $ToxN_{Pa}$ and 17 μg $ToxI_{Pa}$ transcript (total volume 140 μL), and reaction 2 contained 20 μg $ToxN_{Pa}$ and 150 μg $ToxI_{Pa}$ single repeats (total volume 120 μL). All components were in gel filtration buffer. Reactions were incubated at 37 °C for 1 h, diluted to a 200-μL volume in gel filtration buffer, and then were used for size-exclusion chromatography on a Superdex S200 13/30 column (GE Healthcare) at a flow rate 0.6 $mL \cdot min^{-1}$ and a load of 100 μL. Samples analyzed in this way were the two reassembly reactions, $ToxN_{Pa}$, $ToxIN_{Pa}$, $ToxI_{Pa}$ monomer and full $ToxI_{Pa}$ transcript controls, and five size-calibration standards (Table S1).

**$ToxIN_{Bt}$ Purification, Crystallization, and Structure Determination.** $ToxI_{Bt}$ and $ToxN_{Bt}$ were coexpressed in an *E. coli* ER2566 strain (New England BioLabs) carrying the plasmids pFLS67 and pFLS44 (Table S3). Cells were grown at 37 °C to $OD_{600}$ 0.8, and $ToxIN_{Bt}$ complex was expressed overnight following a temperature shift to 18 °C and induction with 1 mM IPTG. Cells were resuspended in 5 mL lysis buffer [500 mM NaCl, 50 mM Tris·HCl, 10 mM imidazole, 10% (vol/vol) glycerol, pH 8.0] per gram of cell mass and were lysed by sonication, and the $ToxIN_{Bt}$ complex was purified using Ni-NTA (Qiagen) $Ni^{2+}$-affinity chromatography followed by HiTrap-Q (GE Healthcare) anion-exchange chromatography with a gradient of 50 mM to 1 mM NaCl. Purified $ToxIN_{Bt}$ complex was concentrated to 6.8 $mg \cdot mL^{-1}$ and was used directly in crystallization trials in its anion-exchange elution buffer (280–300 mM NaCl, 50 mM Tris·HCl, 1 mM DTT, pH 7.5). Initial crystallization screens were performed using vapor diffusion at 18 °C in 96-well sitting-drop plates using JCSG+, Procomplex, Nucleix, and PACT screens (Qiagen), with drop sizes of 100 nL protein plus 100 nL precipitant against a 200-μL reservoir of the same precipitant. Crystallization optimization was performed by conducting manual screens around several of the conditions that produced hits, and crystals diffracting to 2.2 Å were obtained by streak seeding into a 1.2 + 1.2 μL hanging-drop setup with a reservoir of 0.2 M ammonium phosphate, 0.1 M Tris·HCl (pH 8.5), and 50% (vol/vol) 2-methyl-2,4-pentanediol (MPD) (JCSG + screen condition 11).

X-ray diffraction data from a single crystal in spacegroup P6 were collected at wavelength 0.9795 Å at station I02 of the Diamond Light Source, Oxford, UK. Data processing and reduction were performed with iMOSFLM (42), SCALA (43), and TRUNCATE (44) in the CCP4 suite of programs (45). Initial molecular replacement attempts in PHASER (46) with the $ToxIN_{Pa}$ structure [Protein Data Bank (PDB) ID code 2XDB] did not yield a solution, so a $ToxN_{Bt}$ homology model was generated using MODELER. The $toxN_{Pa}$ and $toxN_{Bt}$ sequences were aligned using FUGUE to guide the construction of a modified homology model in COOT (47) based on the $ToxN_{Pa}$ chain in PDB 2XDB, with variable loop regions deleted and nonconserved residues changed to alanine. This search model, which did not contain either heteroatoms or ToxI, was used for molecular replacement (rotation and translation) in PHASER. The initial unbiased Fo-Fc map at 2.5σ (Fig. S3*A*) was calculated from this solution. This map gave positive peaks with a maximum value of 0.7989 electron·$Å^3$ at an rmsd of 6.53 σ, corresponding to the $PO_4^-$ groups of the bound $ToxI_{Bt}$ RNA. The continuous Fo-Fc map allowed portions of the bases and backbone of a consensus $ToxI_{Bt}$ RNA to be traced unambiguously. Following building of the $ToxI_{Bt}$, the $ToxI_{Bt}$:$ToxN_{Bt}$ model was used as the search model for an additional iteration of molecular replacement in PHASER (Table S2). The structure refinement was performed using restrained maximum-likelihood target function, bulk solvent, and anisotropic scaling, and group_TLS (Translation/Libration/Screw) in PHENIX (48). Simulated annealing was used in the early stages to reduce model bias. Water molecules were assigned to positive peaks with a maximum peak height of 0.2107 electron·$Å^3$, with an rmsd in the range of 2.5–4.17 σ in the Fo-Fc map at full occupancy. No positive peaks at rmsd greater than 4.5 σ were observed in the Fo-Fc map, suggesting there were no metal ions present

in the complex at significant occupancy. The stereochemistry of the final structure was checked using SFCHECK and PROCHECK from the CCP4 program suite. The final 2.2-Å structure of the $ToxN_{Bt}$–$ToxI_{Bt}$ complex contains $ToxN_{Bt}$ residues 5–172, 34 nt $ToxI_{Bt}$, and one MPD molecule from the crystallization precipitant (Table S2). Structural superimpositions were done using SUPERPOSE, LSQ, and COOT, and accessible surface areas were calculated using PISA with a probe solvent molecule radius of 1.4 Å. Figures were prepared in PyMOL. Leontis–Westhof symbolism for base pairing (49) was used in the $ToxI_{Bt}$ schematic figure (Fig. 5*B*).

**Identification of RNA Cleavage Sites by 5′ RACE.** *E. coli* K-12 *rpoD, ompF, ompA,* and *dksA* RNAs were transcribed from PCR product templates using T7 RNA polymerase (Fermentas). RNA was added to purified $ToxIN_{Pa}$ or $ToxIN_{Bt}$ in a 1:4 molar ratio and incubated in 50 mM NaCl, 50 mM Tris·HCl, pH 7.5, at 37 °C for 2 h. The cleaved RNA was purified using a NucleoSpin II RNA cleanup kit (Macherey-Nagel). Then 200 ng of treated RNA was reverse transcribed in a SuperScriptII RT (Invitrogen) reaction using up to three gene-specific primers (from FS60, FS62, FS64, FS66, FS68, and FS79–FS96; Table S4). Products then were poly(G)-tailed with TdT terminal transferase (Roche), amplified by PCR using a polyCD forward primer and a gene-specific reverse primer (Table S4), and sequenced. Where sequencing of a PCR product gave an ambiguous result, the product was cloned into pBS KSII+ and sequenced from the recombinant plasmid. Sequence specificity profiles were generated using WebLogo (50).

**ACKNOWLEDGMENTS.** We thank the Beamline scientists at station I02 of the Diamond Light Source, Oxford, United Kingdom for the use of facilities. We also thank Dr. Marko Hyvönen for the use of equipment, and Professor Kenn Gerdes and the Bacillus Genetic Stock Centre for providing plasmids and strains. This work was supported by a grant from the Biotechnology and Biological Sciences Research Council, United Kingdom (to G.P.C.S. and B.F.L.). B.F.L. and X.Y.P. also were supported by the Wellcome Trust. F.L.S. is a Commonwealth Scholar funded by the United Kingdom Department for Business, Innovation and Skills and the Cambridge Commonwealth Trust through the Commonwealth Scholarships Commission, United Kingdom.

1. Storz G, Vogel J, Wassarman KM (2011) Regulation by small RNAs in bacteria: Expanding frontiers. *Mol Cell* 43(6):880–891.
2. Wiedenheft B, Sternberg SH, Doudna JA (2012) RNA-guided genetic silencing systems in bacteria and archaea. *Nature* 482(7385):331–338.
3. Babitzke P, Romeo T (2007) CsrB sRNA family: Sequestration of RNA-binding regulatory proteins. *Curr Opin Microbiol* 10(2):156–163.
4. Wassarman KM (2007) 6S RNA: A small RNA regulator of transcription. *Curr Opin Microbiol* 10(2):164–168.
5. Fozo EM, et al. (2010) Abundance of type I toxin-antitoxin systems in bacteria: Searches for new candidates and discovery of novel families. *Nucleic Acids Res* 38(11): 3743–3759.
6. Leplae R, et al. (2011) Diversity of bacterial type II toxin-antitoxin systems: A comprehensive search and functional analysis of novel families. *Nucleic Acids Res* 39(13):5513–5525.
7. Van Melderen L (2010) Toxin-antitoxin systems: Why so many, what for? *Curr Opin Microbiol* 13(6):781–785.
8. Masuda H, Tan Q, Awano N, Wu K-P, Inouye M (2012) YeeU enhances the bundling of cytoskeletal polymers of MreB and FtsZ, antagonizing the CbtA (YeeV) toxicity in *Escherichia coli*. *Mol Microbiol* 84(5):979–989.
9. Wang X, et al. (2012) A new type V toxin-antitoxin system where mRNA for toxin GhoT is cleaved by antitoxin GhoS. *Nat Chem Biol* 8:855–861.
10. Ogura T, Hiraga S (1983) Mini-F plasmid genes that couple host cell division to plasmid proliferation. *Proc Natl Acad Sci USA* 80(15):4784–4788.
11. Maisonneuve E, Shakespeare LJ, Jørgensen MG, Gerdes K (2011) Bacterial persistence by RNA endonucleases. *Proc Natl Acad Sci USA* 108(32):13206–13211.
12. Fineran PC, et al. (2009) The phage abortive infection system, ToxIN, functions as a protein-RNA toxin-antitoxin pair. *Proc Natl Acad Sci USA* 106(3):894–899.
13. Blower TR, et al. (2009) Mutagenesis and functional characterization of the RNA and protein components of the *toxIN* abortive infection and toxin-antitoxin locus of *Erwinia*. *J Bacteriol* 191(19):6029–6039.
14. Blower TR, et al. (2011) A processed noncoding RNA regulates an altruistic bacterial antiviral system. *Nat Struct Mol Biol* 18(2):185–190.
15. Blower TR, et al. (2012) Identification and classification of bacterial type III toxin-antitoxin systems encoded in chromosomal and plasmid genomes. *Nucleic Acids Res* 40(13):6158–6173.
16. Zhang J, Zhang Y, Zhu L, Suzuki M, Inouye M (2004) Interference of mRNA function by sequence-specific endoribonuclease PemK. *J Biol Chem* 279(20):20678–20684.
17. Zhang Y, et al. (2003) MazF cleaves cellular mRNAs specifically at ACA to block protein synthesis in *Escherichia coli*. *Mol Cell* 12(4):913–923.
18. Kamada K, Hanaoka F (2005) Conformational change in the catalytic site of the ribonuclease YoeB toxin by YefM antitoxin. *Mol Cell* 19(4):497–509.
19. Titok MA, et al. (2003) *Bacillus subtilis* soil isolates: Plasmid replicon analysis and construction of a new theta-replicating vector. *Plasmid* 49(1):53–62.
20. Van der Auwera GA, Andrup L, Mahillon J (2005) Conjugative plasmid pAW63 brings new insights into the genesis of the *Bacillus anthracis* virulence plasmid pXO2 and of the *Bacillus thuringiensis* plasmid pBT9727. *BMC Genomics* 6:103.
21. Blower TR, Salmond GPC, Luisi BF (2011) Balancing at survival's edge: The structure and adaptive benefits of prokaryotic toxin-antitoxin partners. *Curr Opin Struct Biol* 21(1):109–118.
22. Abu Almakarem AS, Petrov AI, Stombaugh J, Zirbel CL, Leontis NB (2012) Comprehensive survey and geometric classification of base triples in RNA structures. *Nucleic Acids Res* 40(4):1407–1423.
23. Schuwirth BS, et al. (2005) Structures of the bacterial ribosome at 3.5 Å resolution. *Science* 310(5749):827–834.
24. Nissen P, Ippolito JA, Ban N, Moore PB, Steitz TA (2001) RNA tertiary interactions in the large ribosomal subunit: The A-minor motif. *Proc Natl Acad Sci USA* 98(9): 4899–4903.
25. Kamphuis MB, et al. (2006) Model for RNA binding and the catalytic site of the RNase Kid of the bacterial *parD* toxin-antitoxin system. *J Mol Biol* 357(1):115–126.
26. Tuerk C, MacDougal S, Gold L (1992) RNA pseudoknots that inhibit human immunodeficiency virus type 1 reverse transcriptase. *Proc Natl Acad Sci USA* 89(15):6988–6992.
27. Gopinath SC, Sakamaki Y, Kawasaki K, Kumar PK (2006) An efficient RNA aptamer against human influenza B virus hemagglutinin. *J Biochem* 139(5):837–846.
28. Gold L, Polisky B, Uhlenbeck O, Yarus M (1995) Diversity of oligonucleotide functions. *Annu Rev Biochem* 64:763–797.
29. Brierley I, Pennell S, Gilbert RJC (2007) Viral RNA pseudoknots: Versatile motifs in gene expression and replication. *Nat Rev Microbiol* 5(8):598–610.
30. Staple DW, Butcher SE (2005) Pseudoknots: RNA structures with diverse functions. *PLoS Biol* 3(6):e213.
31. Ferré-D'Amaré AR, Zhou K, Doudna JA (1998) Crystal structure of a hepatitis delta virus ribozyme. *Nature* 395(6702):567–574.
32. Montange RK, Batey RT (2006) Structure of the S-adenosylmethionine riboswitch regulatory mRNA element. *Nature* 441(7097):1172–1175.
33. Smith KD, Shanahan CA, Moore EL, Simon AC, Strobel SA (2011) Structural basis of differential ligand recognition by two classes of bis-(3′-5′)-cyclic dimeric guanosine monophosphate-binding riboswitches. *Proc Natl Acad Sci USA* 108(19):7757–7762.
34. Sussman D, Nix JC, Wilson C (2000) The structural basis for molecular recognition by the vitamin B 12 RNA aptamer. *Nat Struct Biol* 7(1):53–57.
35. Haurwitz RE, Sternberg SH, Doudna JA (2012) Csy4 relies on an unusual catalytic dyad to position and cleave CRISPR RNA. *EMBO J* 31(12):2824–2832.
36. Brouns SJ, et al. (2008) Small CRISPR RNAs guide antiviral defense in prokaryotes. *Science* 321(5891):960–964.
37. McKenzie JL, et al. (2012) A VapBC toxin-antitoxin module is a posttranscriptional regulator of metabolic flux in mycobacteria. *J Bacteriol* 194(9):2189–2204.
38. Winther KS, Gerdes K (2011) Enteric virulence associated protein VapC inhibits translation by cleavage of initiator tRNA. *Proc Natl Acad Sci USA* 108(18):7403–7407.
39. Zhu L, et al. (2008) The mRNA interferases, MazF-mt3 and MazF-mt7 from *Mycobacterium tuberculosis* target unique pentad sequences in single-stranded RNA. *Mol Microbiol* 69(3):559–569.
40. Guzman LM, Belin D, Carson MJ, Beckwith J (1995) Tight regulation, modulation, and high-level expression by vectors containing the arabinose pBAD promoter. *J Bacteriol* 177(14):4121–4130.
41. Christensen-Dalsgaard M, Gerdes K (2006) Two *higBA* loci in the *Vibrio cholerae* superintegron encode mRNA cleaving enzymes and can stabilize plasmids. *Mol Microbiol* 62(2):397–411.
42. Battye TGG, Kontogiannis L, Johnson O, Powell HR, Leslie AGW (2011) iMOSFLM: A new graphical interface for diffraction-image processing with MOSFLM. *Acta Crystallogr D Biol Crystallogr* 67(Pt 4):271–281.
43. Evans P (2006) Scaling and assessment of data quality. *Acta Crystallogr D Biol Crystallogr* 62(Pt 1):72–82.
44. French S, Wilson K (1978) On the treatment of negative intensity observations. *Acta Crystallogr A* 34:517–525.
45. Winn MD, et al. (2011) Overview of the CCP4 suite and current developments. *Acta Crystallogr D Biol Crystallogr* 67(Pt 4):235–242.
46. McCoy AJ, et al. (2007) Phaser crystallographic software. *J Appl Cryst* 40(Pt 4):658–674.
47. Emsley P, Lohkamp B, Scott WG, Cowtan K (2010) Features and development of Coot. *Acta Crystallogr D Biol Crystallogr* 66(Pt 4):486–501.
48. Adams PD, et al. (2010) PHENIX: a comprehensive Python-based system for macromolecular structure solution. *Acta Crystallogr D Biol Crystallogr* 66:213–221.
49. Leontis NB, Westhof E (2001) Geometric nomenclature and classification of RNA base pairs. *RNA* 7(4):499–512.
50. Crooks GE, Hon G, Chandonia J-M, Brenner SE (2004) WebLogo: A sequence logo generator. *Genome Res* 14(6):1188–1190.